PLOS ONE

RESEARCH ARTICLE

Unconstrained coevolution of bacterial size and the latent period of plastic phage

Juan A. Bonachela[1]*, **Melinda Choua**[2], **Michael R. Heath**[3]

1 Department of Ecology, Evolution, and Natural Resources, Rutgers University, New Brunswick, NJ, United States of America, **2** Blue Remediation Ltd., Glasgow, Scotland, United Kingdom, **3** Marine Population Modelling Group, Department of Mathematics and Statistics, University of Strathclyde, Glasgow, Scotland, United Kingdom

* juan.bonachela@rutgers.edu

Citation: Bonachela JA, Choua M, Heath MR (2022) Unconstrained coevolution of bacterial size and the latent period of plastic phage. PLoS ONE 17(5): e0268596. https://doi.org/10.1371/journal.pone.0268596

Editor: Claude Loverdo, Sorbonne Université Campus Pierre et Marie Curie: Sorbonne Universite Campus Pierre et Marie Curie, FRANCE

Received: December 15, 2021

Accepted: May 2, 2022

Published: May 26, 2022

Data Availability Statement: No relevant data other than the equations above were used in this research. Code used to implement such equations are available at: 10.17605/OSF.IO/B594F.

Funding: JAB was supported by a grant from the Simons Foundation (award #826106); MC and MRH were supported to varying extents by the Marine Alliance for Science and Technology for Scotland (MASTS) pooling scheme, Scottish Funding Council grant reference HR09011.

Abstract

Viruses play critical roles in the dynamics of microbial communities. Lytic viruses, for example, kill significant fractions of autotrophic and heterotrophic microbes daily. The dynamic interplay between viruses and microbes results from an overlap of physiological, ecological, and evolutionary responses: environmental changes trigger host physiological changes, affecting the ecological interactions of host and virus and, ultimately, the evolutionary pressures influencing the two populations. Recent theoretical work studied how the dependence of viral traits on host physiology (viral plasticity) affects the evolutionarily stable host cell size and viral infection time emerging from coevolution. Here, we broaden the scope of the framework to consider any coevolutionary outcome, including potential evolutionary collapses of the system. We used the case study of *Escherichia coli* and T-like viruses under chemostat conditions, but the framework can be adapted to any microbe-virus system. Oligotrophic conditions led to smaller, lower-quality but more abundant hosts, and infections that were longer but produced a reduced viral offspring. Conversely, eutrophic conditions resulted in fewer but larger higher-quality hosts, and shorter but more productive infections. The virus influenced host evolution decreasing host size more noticeably for low than for high dilution rates, and for high than for low nutrient input concentration. For low dilution rates, the emergent infection time minimized host need/use, but higher dilution led to an opportunistic strategy that shortened the duration of infections. System collapses driven by evolution resulted from host failure to adapt quickly enough to the evolving virus. Our results contribute to understanding the eco-evolutionary dynamics of microbes and virus, and to improving the predictability of current models for host-virus interactions. The large quantitative and qualitative differences observed with respect to a classic description (in which viral traits are assumed to be constant) highlights the importance of including viral plasticity in theories describing short- and long-term host-virus dynamics.

Competing interests: The authors have declared that no competing interests exist.

Introduction

Viruses are the most abundant biological entities on Earth, yet cannot replicate without the synthesis machinery of a cellular host [1]. This dependence between viral replication and host is evident in the description of the infection cycle of lytic phages [2]. The lytic cycle starts when freely diffusing viruses encounter a host and attach to receptors at the cell surface. The virus then injects its genetic material into the host and hijacks the synthesis machinery to produce the components of what will be the new virions. Virions are then assembled and, finally, the expression of the holin gene leads to the perforation of the cell membrane and cell lysis, releasing the viral offspring into the medium. Key reproduction-limiting steps in the lytic cycle are the adsorption rate of viruses onto host receptors, duration of the synthesis (or eclipse) period and the virion assembly period, and the burst size (or offspring number). The time between adsorption and lysis is referred to as the latent period. Although it is still unclear what triggers lysis, all things being equal longer infection times should result in larger viral production [3].

The intertwinement between every single stage of the viral lytic infection and host metabolism and machinery [4] means that the host physiological state necessarily influences the value of these important viral traits, and therefore viral performance [5–10]. This dependence of viral traits on host physiology (viral plasticity hereon), observed across systems, has been quantified systematically for the bacterium *Escherichia coli* and T viruses using host growth rate as a measure of physiological state [5–8]. Moreover, the qualitative shape of the dependence of viral traits on host growth rate seems to be conserved across different strains of *E. coli* and T viruses, as well as different experimental conditions [11], thus suggesting that these functional forms stem from fundamental mechanisms generically present across systems.

In spite of the importance of viral plasticity, only recently have theories started to take it into account when exploring host-virus dynamics from an ecological [11–13] or an evolutionary perspective [11, 14, 15].

From an ecological point of view, considering viral plasticity leads to the counterintuitive result that lower nutrient conditions are somewhat beneficial for the host, as the consequent deterioration in physiological state is compensated by the associated decrease in viral performance and reduced viral pressure [11]. From an evolutionary point of view, we recently explored how viral plasticity affects the coevolution of host size and viral latent period [14]. Our results, restricted to evolutionarily stable states in which both host and virus coexist, showed that such coevolution leads to a negative correlation between host size and viral latent period. Poor growth conditions for the host selected for small sizes and long infections, whereas good growth conditions selected for large hosts and short infections. For all growth conditions, host size resulting from coevolution was larger than in the absence of the virus, and the viral latent period was longer than if hosts did not evolve. Here, we revisit the system to expand our theoretical framework and explore a wider range of potential evolutionary outcomes, including the possibility for evolutionary branching (trait evolution leading to stable coexistence of several host or virus phenotypes) and the possibility for coevolution to drive either host or virus to extinction (evolutionary collapses).

We aim to understand the mechanisms underlying the different outcomes of the host-virus dynamics represented in our model, and the role played by viral plasticity. These dynamics are highly nontrivial, as short generation times and vast populations of both host and virus lead to rapid evolution that, ultimately, may trigger interactions between ecological and evolutionary timescales (eco-evolutionary dynamics) [16, 17]. Thus, we will pay special attention to the coevolutionary transient, i.e. the evolutionary path leading to such outcomes. We also extend our framework to consider a larger variance for the evolutionary step, which ensures the

robustness of the evolutionary equilibrium reached by the system. In addition, we include viral avoidance of secondary infection by other viral individuals (superinfection), which not only does it increase the realism of the framework but also increases its dynamical stability by reducing the amplitude of the antagonistic demographic oscillations that characterize populations in host-virus systems. These modifications to the model aim to ensure that more replicates reach a meaningful outcome that results from the eco-evolutionary dynamics between host and virus, thus increasing the breadth and robustness of our study.

As in the previous version of the model, we will focus on cell radius (generically, cell size) as the evolving trait for the host, and latent period as the evolving trait for the virus. As justified below in detail, size is a "master trait" for microbes (e.g. [18]) that influences every aspect of their physiology and ecological interactions, thus affecting most other host traits. On the other hand, the latent period is one of the most important life-history traits for the virus, and an ideal trait to study in an evolutionary framework given the small pleiotropic effects on other traits [19].

Understanding not only stable coexistence but also branching and collapse, and how those equilibria were reached, can potentially provide key information about a variety of systems. For example, it can help us understand the eco-evolutionary dynamics governing phytoplankton blooms ("boom and bust" events occurring in Spring –and sometimes Fall– due to increased daylight and readily available nutrients), which end with very low phytoplankton densities or even collapse, an outcome in which viruses play a prominent role [20, 21]. Including plasticity can improve the dynamic description of other viral-mediated processes that are key for biogeochemical cycles and microbial diversity (e.g. viral shunt and shuttle) [20, 22, 23], and therefore the reliability of models that estimate primary production. The dynamics, and not only the end result, may also be of relevance to the design of anti-bacterial treatments (phage therapy [24]), or when studying viral infections of changeable communities such as the animal microbiome. Finally, including viral plasticity can be key to reliably representing the viral infection of biofilms, groups of bacteria attached to each other and a surface by a polymeric matrix with complex shapes, thus characterized by a very variable (temporal and spatial) distribution of nutrient availability that leads to a mosaic of growth conditions within and around the biofilm [25, 26].

Methods

To explore the unconstrained coevolutionary dynamics of host and virus, we used a standard delay model that has been shown to produce realistic ecological and evolutionary behavior [11, 27, 28]. This model describes the dynamics of the population of uninfected hosts (C, in $cell \cdot l^{-1}$), infected hosts (I, in $cell \cdot l^{-1}$), free viruses (V, in $ind \cdot l^{-1}$), and the concentration of the most limiting nutrient for the host (N, in $mol \cdot l^{-1}$), all interacting in a chemostat environment:

$$\frac{dC(t)}{dt} = \mu(N)\, C - kCV - \alpha C C_{all} - w_{out} C \tag{1}$$

$$\frac{dI(t)}{dt} = kCV - kC_{t-L}V_{t-L}\, e^{-w_{out}L} - w_{out} I \tag{2}$$

$$\frac{dV(t)}{dt} = B\, kC_{t-L}V_{t-L}\, e^{-w_{out}L} - kCV - \alpha_V V V_{all} - mV - w_{out} V \tag{3}$$

$$\frac{dN(t)}{dt} = w_{in}N_0 - w_{out}N - \mu(N)C/Y. \tag{4}$$

Table 1. Symbols for variables used in the model and parameter values. Data for the host obtained from various *E. coli* experiments [40–42], as is the case for host trade-off functions and their parametrizations [34, 37, 38]; data for the virus into the ranges shown/used in experiments [43–45] and data that informed previous theoretical work [46]. For the calculation of the yield factor from the references, we assumed a fixed carbon content per host cell of 10^{-12} *g*. For other conversions, we used that the carbon content of glucose is 180.15588 $mol \cdot mol^{-1}$.

Symbol	Description	Units	Value
L	Latent period	d	Evolutionary variable
r	Host cell radius	$\mu meter$	Evolutionary variable
C	Density noninfected host	$cell \cdot l^{-1}$	Eq (1)
I	Density infected host	$cell \cdot l^{-1}$	Eq (2)
V	Density free virus	$ind. \cdot l^{-1}$	Eq (3)
N	Glucose concentration	$mol \cdot l^{-1}$	Eq (4)
μ	Host growth rate	d^{-1}	Eq (5)
μ_{max}	Maximum growth rate for host	d^{-1}	Eq (6)
K_N	Half-saturation constant for growth	$mol \cdot l^{-1}$	Eq (8)
k	Adsorption rate	$l \cdot cell^{-1} \cdot d^{-1}$	Eq (7)
B	Burst size	$virions$	Eq (9)
E	Eclipse period	d	Eq (10)
M	Maturation rate	$virions d^{-1}$	Eq (11)
$\mu_{max_{exp}}$	Max. host growth rate from experiments	d^{-1}	40.8
$\mu_{max_{ref}}$	Saturating max. growth rate in Eq (8)	d^{-1}	28.8
$K_{N_{ref}}$	Half-saturation constant at $\mu_{max} = 0$	$mol \cdot l^{-1}$	$3.55 \cdot 10^{-8}$
D_0	Diffusivity T-like viruses in water	$dm^2 \cdot d^{-1}$	$3.73 \cdot 10^{-5}$
Y	Yield parameter	$cell mol^{-1}$	9×10^{13}
m	Virus mortality rate	d^{-1}	0.09
N_0	Glucose input/supply concentration	$mol \cdot l^{-1}$	$3 \cdot 10^{-6}, 5 \cdot 10^{-6}, 10^{-5}, 5 \cdot 10^{-5}, 10^{-4}$
w_{out}	Chemostat dilution rate	d^{-1}	$0.05\mu_{max_{ref}} - 0.55\mu_{max_{ref}}$
w_{in}	Chemostat inflow rate	d^{-1}	w_{out}
a	Factor of Eq (6)	$d^{-1} \cdot \mu m^{-3p}$	$(24 \cdot 10^{-12}) \cdot 10^{1.9}$
p	Exponent of Eq (6)	(-)	0.177
dr	Min. difference in r for host phenotypes	$\mu meter$	0.01
dL	Min. difference in L for viral phenotypes	d	0.003472
σ_r	Std. dev. host evolutionary step	$\mu meter$	$2dr = 0.02$
σ_L	Std. dev. viral evolutionary step	d	$2dL = 0.00694$

https://doi.org/10.1371/journal.pone.0268596.t001

See Table 1 for symbols and units. The population of uninfected hosts increases thanks to the uptake of the most limiting nutrient (here, glucose; first term, Eq (1)), declines due to infection (second term) or dilution from the chemostat (last term). Similarly to [14], we consider here potential competition for space, light, or other resources not explicitly modeled that can affect negatively the growth of the focal population (third term), a plausible scenario as the framework introduces in ecological time new host mutants (see below); here, C_{all} represents all hosts from all phenotypes in the system. The population of infected individuals increases due to infection (first term, Eq (2)), and declines when infected cells are diluted (third term) or lysed (second term). Note that the number of cells that are lysed at time t were infected a latent period L in the past, and thus this lysis term considers the number of infections at time $t - L$ weighted by the probability of surviving dilutions in that period ($e^{-w}{}_{out}\, L$). Cells lysed at time t produce the new batch of viruses (first term of Eq (3)), and the population declines as viruses infect new hosts (second term), decay (become non-infective after a period of time, fourth term), or are diluted from the chemostat (last term). We expanded the model from [14] to

include also the possibility for phage to avoid superinfection, thus accounting for the battery of mechanisms that a phage that has entered the host can deploy to prevent any other virus from using the same host for replication [29]; this mechanism, here implemented with a density-dependent term (third term, where V_{all} represents the sum of all viral density across phenotypes), is not only more realistic but also reduces the mathematical instability reported in [13, 14]. Finally, the dynamics of the most limiting nutrient (glucose) include the inflow and dilution of nutrient that characterize the chemostat environment (first and second terms), and the uptake of the nutrient by the uninfected hosts (last term). We assumed that cell growth and replication stop at infection, and thus infected cells do not take up glucose nor they need to be considered for the density-dependent term (third term) in Eq (1). Nutrient uptake is calculated based on requirement for growth, with the growth rate given by the classic Monod formulation [30]:

$$\mu = \mu_{max}(r)\frac{N}{N + K_N}, \tag{5}$$

where μ_{max} is the maximum growth rate (in d^{-1}), and K_N (in $mol \cdot l^{-1}$) the half-saturation constant for growth on nutrient N.

Following standard modeling practice, we set a threshold below which either the total host (i.e. infected and uninfected cells) or the free viral population are considered to be extinct. This practice prevents unrealistically low values of the population densities from "regenerating" populations. Here, we set a threshold of 1 $ind \cdot l^{-1}$ for either population. Differently from [14], we consider that the threshold for the virus includes not only free viruses but also replicating viruses (i.e. viruses that are currently infecting a host), which prevents the elimination of viral mutant populations that entered the system recently and are still inside infected cells as part of their first lytic cycle. Neither reverting this more conservative rule, nor eliminating the new superinfection avoidance term in Eq (3), altered qualitatively our results.

Traits and trade-offs

Although the model above can be applied to any bacteria-phage system, for the sake of concreteness here we consider the dynamics of one of the most studied examples: T phage infecting *Escherichia coli*. See Table 1 for parameter values.

As explained in detail in the next section, we focus on size as single evolutionary trait for the host. The choice is justified because, for microbial organisms, size is linked to almost every aspect of its life cycle and ecological functioning (e.g. [18, 31]). Particularly for *E. coli*, this evolvable trait [32, 33] has been shown to be positively correlated with the maximum growth rate [34]:

$$\mu_{max}(r) = a\left[\frac{4}{3}\pi(10^{-4}r)^3\right]^p, \tag{6}$$

where we used the spherical approximation for the cell, r is cell radius (in microns), and a and p are parameters shaping this power-law correlation (see Table 1 for values and units). Cell size also affects the rate of encounters with the virus, which can be accounted for using the following expression for the adsorption rate, k (in $l \cdot d^{-1}$) [35]:

$$k(r) = 4\pi D_0 10^{-5} r, \tag{7}$$

with D_0 (in $dm^2 \cdot d^{-1}$) the diffusivity of T-like viruses in water. Since T viruses use lipopolysaccharides (LPS) as main target receptors for adsorption to the *E. coli* cell, and LPS are very

abundant on the cell surface (more than 75% coverage) [36], we assumed for simplicity that all encounters led to a successful adsorption.

In addition, we considered the following correlation between the half-saturation constant for growth and the maximum growth rate [37, 38]:

$$K_N = K_{N_{ref}} e^{\frac{\mu_{max}(r)}{\mu_{max_{ref}} - \mu_{max}(r)}}, \tag{8}$$

which effectively links the half-saturation constant with size as well. Thus, large cell sizes lead to high growth potential but low affinity (inverse of K_N), therefore setting a tradeoff for the host. The parameter $\mu_{max_{ref}}$ represents a maximum value for μ_{max}, and $K_{N_{ref}}$ is the half-saturation value for $\mu_{max} = 0$ (see Table 1 for values).

Together with the adsorption rate k above, the main viral traits that define the infection cycle are the eclipse period, E (in d), the maturation rate, M (in $virion \cdot d^{-1}$), the burst size, B (in $virion \cdot cell^{-1}$), and the latent period, L (in d). Here, we considered the latter the focus of viral evolution, since it determines the timing of lysis and limits virion production by setting a maximum time for synthesis and assembly [10]. Such a limitation results in a correlation between burst size and latent period, under the assumption that the timing to exhaust intracellular resources is longer than the timing of lysis [3]:

$$B = M \cdot (L - E). \tag{9}$$

As explained above, these viral traits are affected by the host physiological state. Here, we used the host growth rate to represent the cell's physiological state because light, temperature, nutrient availability, and other factors affecting host physiology are ultimately reflected in changes in growth rate. This variable has been used in the past to study how T viruses respond to changes in host physiology by exploring how the value of different viral traits depends on host growth rate [5–8]. An effort to characterize these relationships across *E. coli*-T phage systems showed that the eclipse period can be expressed as [11]:

$$E(\mu) = E_\infty + E_0 e^{-\alpha_E \mu/\mu_{exp}}, \tag{10}$$

and the maturation rate as:

$$M(\mu) = \frac{M_\infty}{1 + e^{-\alpha_M(\mu/\mu_{exp} - M_0)}}. \tag{11}$$

In short, the eclipse period decreases and the maturation rate increases as a function of host growth rate. The maturation rate increases as a sigmoid and reaches a plateau for high host growth rates. The eclipse period decreases exponentially from a non-zero maximum value for $\mu \to 0$ to a minimum value for $\mu \to \mu_{exp}$. The latter is the maximum growth rate observed in the experiments of reference [6] (see Table 1). The former indicates the possibility for phage to replicate even for negligible host growth, which has been observed experimentally for this system [7]. Here, we focused on obligate lytic viruses only, but an alternative strategy for the virus in such challenging conditions is to use a temperate replication mode and switch to lytic mode when appropriate (e.g. [39]). We refer to [11] for further details and biological justification of these functional forms.

From Eqs (10) and (11), it follows that the burst size will be affected by the host growth rate (Eq (9)), which has been observed experimentally in the past (e.g. [8]). The timing of lysis is also influenced by host physiological state; since L is the focus of viral evolution here, however, we let coevolution with the host determine its value and how it depends on the host growth rate.

In contrast, models that do not consider viral plasticity use fixed values for the viral traits above, typically obtained from experiments in which the host is grown at optimal conditions [5]. To study the effect that accounting for plasticity has on standard predictions for host-virus dynamics, in previous work we parametrized the nonplastic case by setting viral traits to their value for best growth physiological status, i.e. by using Eqs (10) and (11) with $\mu = \mu_{max}$ [11, 13, 14]. In [14], however, host maximum growth rate was affected by the evolution of host size; thus, although setting $\mu = \mu_{max}(r)$ was technically consistent with the fact that nonplastic parametrizations rely on "best host growth" values, it somewhat allowed for a form of viral plasticity because the same viral population infecting different host phenotypes (i.e. with different r) would show different trait values. Here, we ensured that the nonplastic case fulfills both aspects of the definition above by using Eqs (10) and (11) with the maximum value for the host growth rate allowed by the tradeoff expression, Eq (8). In other words, $E_{non} = E(\mu_{max_{ref}})$, $M_{non} = M(\mu_{max_{ref}})$, and $B_{non} = M_{non}(L - E_{non})$, which ensures fixed traits for a given viral phenotype regardless of the host it infects.

Evolutionary dynamics

We embedded the model above in an evolutionary framework that has been successfully used in the past to study various aspects of microbial evolution (e.g. [11, 28, 47]). Differently from other traditional evolutionary frameworks, this framework does not impose a separation of the ecological and evolutionary timescales. Instead, it allows for mutations to occur at random times, and thus for new mutant phenotypes to be introduced in the system at ecological timescales.

Our focus on host size and viral latent period as only evolving traits means that these traits characterize host and viral phenotypes, respectively. Thus, all host phenotypes were identical except by their size (and related traits, Eqs (6) and (8)); similarly, given a host growth rate, viral phenotypes only differed in the value of the latent period (and, thus, the burst size, Eq (9)).

The system was initialized with a single host and viral phenotype using a random value for size r and latent period L, respectively. These initial populations interacted through Eqs (1) and (4). At mutation events, the mutating phenotype was selected at random following a roulette-wheel algorithm in which the phenotype with the highest population density (hereon "dominant phenotype", for either host or virus) had the highest probability to be chosen. Thus, a population of a new phenotype was introduced whose trait values were identical to those of the parent except for the evolving (and related) traits. The mutant's value for the evolving trait was chosen at random following a Gaussian distribution centered around the value of the parental trait, and standard deviation given by σ_r (for the host) or σ_L (for the virus). We assumed that two phenotypes were different only if the new value of the trait differed from any existing phenotype an amount dr (for the host) or dL (for the virus); thus, we set the standard deviation for evolutionary steps to be $\sigma_r = 2dr$ and $\sigma_L = 2dL$. This choice allowed for an evolutionary step that was much less restrictive than the one used in [14], which enabled a more efficient and complete exploration of the trait space, yet was sufficiently small for the new phenotype to still be considered a mutation from the parental phenotype. Setting a fixed mutation time for host and virus (either comparable, or with the virus mutating faster than the host), did not alter qualitatively our results but changed the number of competing phenotypes at any given time.

To understand the role of environmental factors on the coevolutionary outcome, we explored different values of both the nutrient input concentration, N_0, and the dilution rate, w. For the latter, we used fractions of the maximum possible growth rate in the system, set by

$\mu_{max_{ref}}$ (see Table 1). In addition, to understand to what extent the coevolutionary behavior of the host resulted from bottom-up versus top-down regulation (i.e. regulated by nutrient availability and uptake vs. regulated by mortality due to the virus, respectively), we compared the host size emerging from coevolution with results obtained in the absence of viruses. The latter provided a reference for evolutionary behavior in response to purely bottom-up processes (in this case, the availability and uptake of glucose). Moreover, we compared the latent periods emerging from coevolution with those obtained in the absence of host evolution. For the latter, we used an analytical expression for the optimal latent period obtained under the assumption that host does not evolve and viral evolution aims to minimize "host use", as per resource competition theory [11, 48] (see S1 File). This comparison allowed us to explore under which environmental conditions the viral strategy departed from "host density minimization" due to host coevolution.

We further assumed that all viruses can infect all hosts. This simplifying assumption was justified by the observation that the coevolution of bacteria and phage can lead to the emergence of generalist viruses [49]. Another potential outcome of coevolution is the possibility for the virus to lyse all available hosts after, e.g. a "host immunity" vs. "viral immunity-avoidance" arms race [50], an example of evolutionary suicide through Tragedy of the Commons [51]. We investigated whether host extinction due to either an "evolutionarily underperforming" host or "evolutionarily overachieving" virus could happen through the coevolution of host size and viral latent period. Thus, in addition to the replicates that resulted in the coexistence of a clear dominant host and virus phenotype [14], we also analyzed the cases in which extinction occurred after a minimum number of days, set to 1, 000 days. Because all replicates start with one random pair of host and virus phenotypes, setting a conservative minimum period of survival for the system filters extinctions occurring due to an unstable initial condition [13] instead of due to evolutionary dynamics.

Our simulations used a forward Euler integration scheme with a time step $dt = 10^{-3}\ d$ (i.e. $1.44 mins$), which is both simple and easy to customize to accommodate the delay terms and other modifications needed to implement the eco-evolutionary dynamics explained above.

Results

Our model represents the dynamics of an evolving host that feeds on glucose, and is lysed by an evolving virus whose performance depends on the physiological state of the host (viral plasticity). Our eco-evolutionary framework allowed for the overlapping and mutual interaction of host-virus coevolution and viral plasticity. Due to the stochastic nature of the replicates (from the initial condition to the random exploration of the trait space for both host and virus), the results below consider instances among 300 replicates that were classified according to whether a dominant host and virus phenotype coexisted at maximum time of the replicate (30, 000 days), or extinction occurred after 1, 000 days. Replicates showing the remaining option (extinction occurring before the minimum number of days) were rejected as the result of a pathological random combination of initial host and virus phenotypes.

Host-virus coexistence

The number of replicates that showed coexistence increased with the input concentration (N_0) for the plastic case, but decreased for the classic parametrization in which viral traits are fixed ("nonplastic case" hereon). Both consistently showed such surviving runs for $N_0 \sim 5 \cdot 10^{-6}$–$10^{-5}\ mol \cdot l^{-1}$. In these surviving replicates, the stochastic exploration of the trait space by both host and phage led to an evolutionarily stable strategy (ESS) given by a value for both evolving traits, host size and viral latent period. Fig 1 shows an example of how the

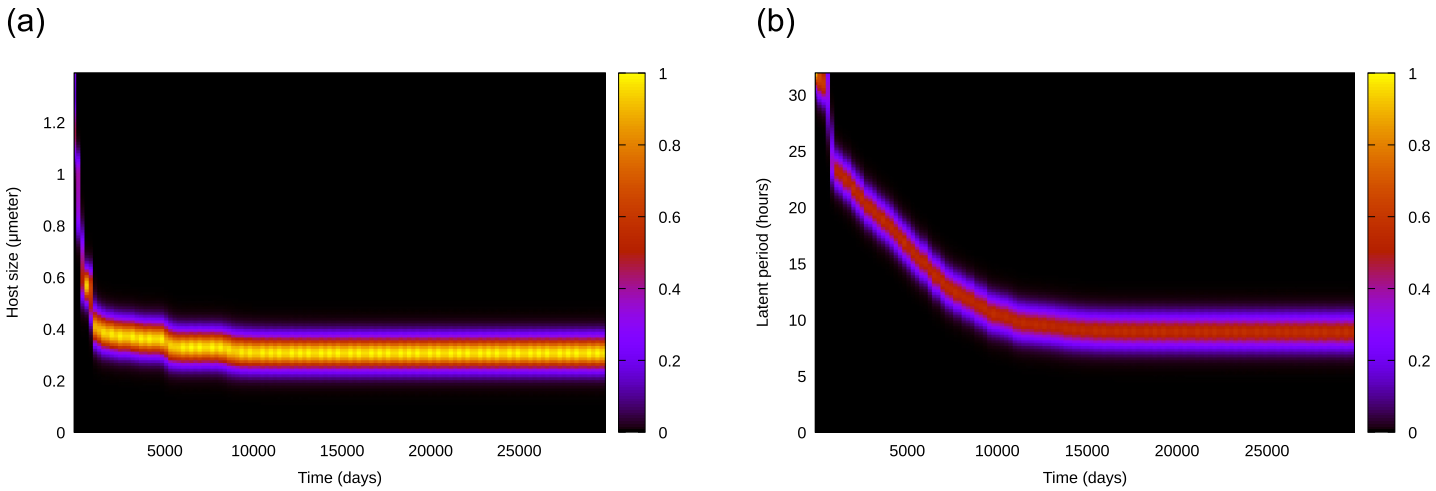

Fig 1. Density plot obtained with the abundance distribution at each time for all host (left) and virus (right) phenotypes, with color representing normalized density. Each population is composed of a clear dominant phenotype (value of host radius and viral latent period, respectively), and others with similar trait values. Both populations reach a stationary state that enables the definition of an evolutionarily stable strategy (ESS) for both evolving traits. Simulations obtained for the plastic case with $w = 0.1\mu_{max_{ref}} = 2.88\ d^{-1}$ and $N_0 = 10^{-5}\ mol \cdot l^{-1}$.

https://doi.org/10.1371/journal.pone.0268596.g001

distribution of abundances for host (left panel) and phage (right panel) phenotypes changed over time. Both host and virus show a distribution (i.e. non-negligible variance in trait value) with a well-defined dominant phenotype, and alternation of dominance over time until reaching a stationary state. Such a stationary state may show demographic oscillations, especially for high input concentration N_0 or the nonplastic case (not shown). Thus, a well-defined evolutionary stationary state was reached for all surviving replicates in spite of the standard deviation for evolutionary steps, σ_r and σ_L, being set to twice the minimum trait difference characterizing phenotypes (dr and dL, see Methods and Table 1), emphasizing the stability of the evolutionary steady state. Fig 1 shows that the host size reached its evolutionary stationary value by following more abrupt changes and fewer alternations of dominance than the viral latent period; in addition, the host trait reached its stationary value before the viral trait, which seemed to be generally the case. The overwhelming dominance of the most abundant phenotype at the stationary state facilitated the selection of the dominant as representative of that replicate (in Fig 1, $(r, L) = (0.98, 0.09)$).

Due to the stochastic character of the eco-evolutionary dynamics, the stationary trait values reached across replicates were not identical. Nonetheless, a representation of the abundance of all phenotypes collected at the end of each replicate (heatmap in Fig 2) showed that the final host and viral populations were mostly composed of a single dominant with a trait value that was similar across replicates. Thus, we did not observe evolutionary branching. In addition, we independently calculated the trait value representing the ESS for the particular environmental conditions (i.e. for a given nutrient input N_0 and dilution rate w). To this end, we selected each replicate's final dominant host and virus by calculating, for each phenotype, the median of their abundance in the last 100 days of the simulation, and identifying the phenotype with the highest median. We then calculated the ESS for the given N_0 and w by averaging across replicates the trait value of the dominant. As the points in Fig 2 show, these average size and latent period (r_{ESS}, L_{ESS}) matched the most abundant trait combinations observed across replicates.

We next explored how the ESS was influenced by environmental conditions. The emergent host size, r_{ESS}, was positively correlated with the dilution rate, opposite to the emergent latent

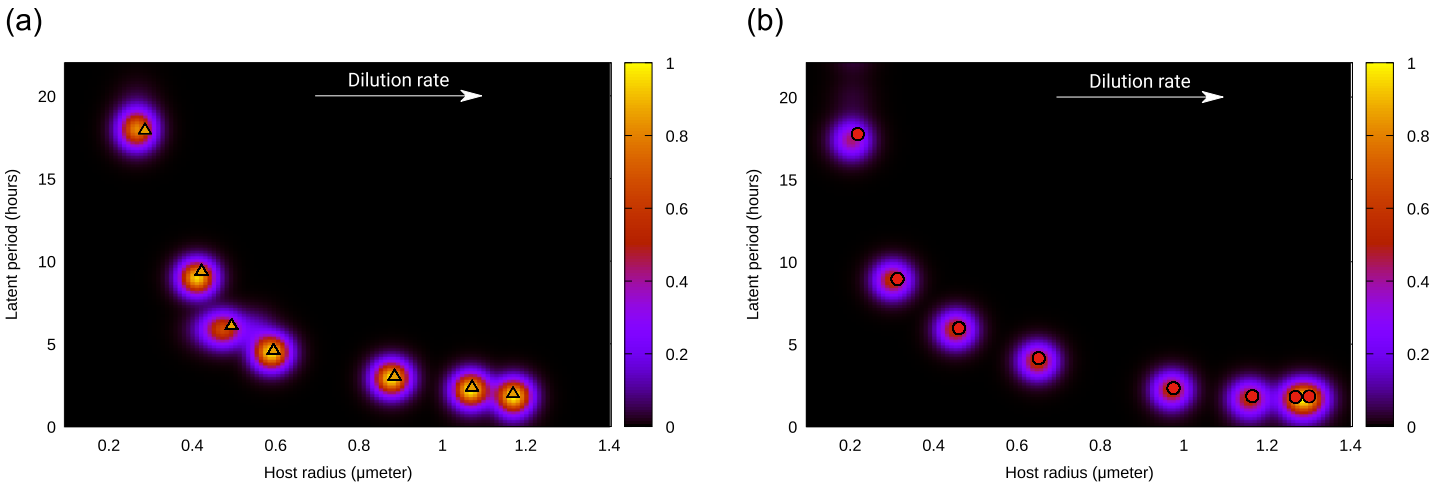

Fig 2. (Normalized) density plots for the final state of the system (heatmap) and average value for traits, (r_{ESS}, L_{ESS}) (points), for different dilution rates, *w*. Left panel, for nutrient input concentration $N_0 = 5 \cdot 10^{-6}\ mol \cdot l^{-1}$; right panel, for $N_0 = 10^{-5}\ mol \cdot l^{-1}$. Both panels, obtained for the plastic case, show the dominance of one well-defined value for host and viral traits.

https://doi.org/10.1371/journal.pone.0268596.g002

period, L_{ESS} (S1 Fig in S1 File). For the former, a higher input concentration, N_0, led to noticeably higher sizes only for high dilution rates *w*; the external nutrient input also somewhat increased the slope of this correlation, and thus for low dilution rates the host radius emerging under low N_0 was slightly larger than under high N_0. The input concentration decreased the emergent latent period. In the nonplastic case, hosts showed a smaller size and viruses showed a smaller latent period than the plastic case, especially for low *w*. Thus, for both plastic and nonplastic cases, the ESS for host size r_{ESS} was inversely correlated with the ESS for viral latent period L_{ESS}, and such r_{ESS} vs. L_{ESS} curve shows a down-left shift for the nonplastic case (Fig 3, left). N_0 barely affected this relationship qualitatively nor quantitatively.

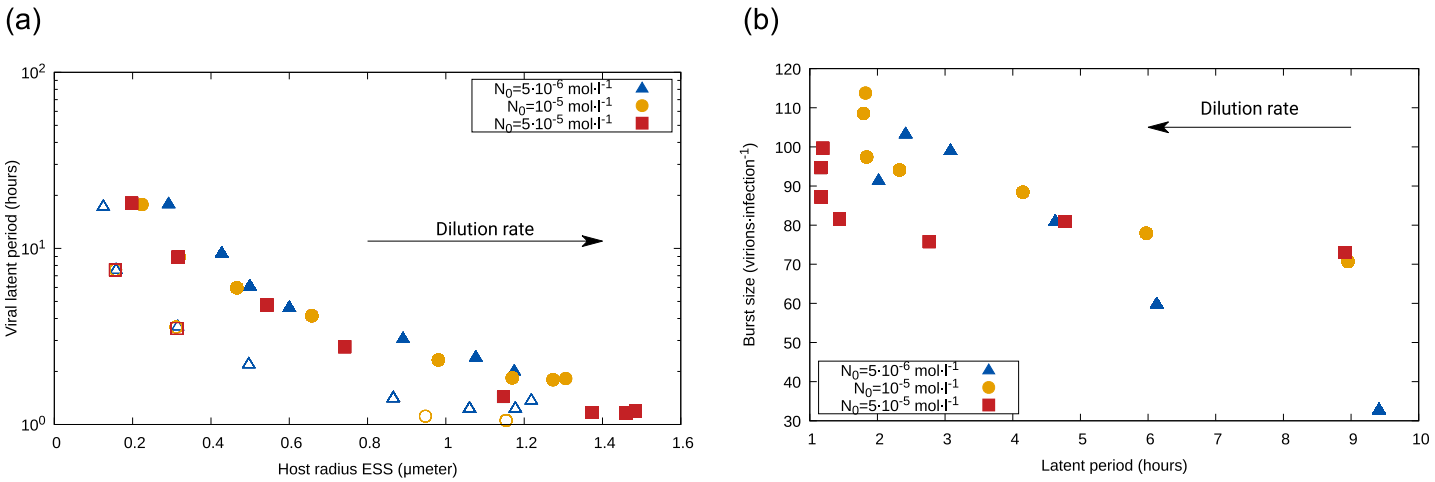

Fig 3. Average across replicates for different traits and cases. Left: Dominant host radius versus dominant latent period; both plastic (full symbols) and nonplastic (open symbols) cases show a negative correlation between r_{ESS} and L_{ESS}, but smaller hosts and shorted infections dominate in the nonplastic case. See S1 Fig in S1 File for trait dependence with dilution rate, *w*, and S5 Fig in S1 File for other versions of the model. Right: Dominant burst size versus dominant latent period, showing a negative correlation between B_{ESS} and L_{ESS} for the plastic case that becomes steeper as N_0 increases. Warmer colors indicate increased input concentrations; the arrow indicates higher dilution, *w*. See S3 Fig in S1 File for nonplastic case and dependence of B_{ESS} on r_{ESS}.

https://doi.org/10.1371/journal.pone.0268596.g003

Next, we focused on the potential tradeoff between viral offspring and latent period. As explained in Methods, viruses in the nonplastic case are characterized by constant eclipse period E and maturation rate M (S2 Fig in S1 File), which leads to a constant burst size B as well (Eq (9)). As a consequence, the relationship between the viral latent period and burst size showed an opposite correlation for the plastic and nonplastic cases (Fig 3, right panel, and S3 Fig in S1 File, left). The latter conserved the classic positive correlation (and therefore tradeoff) between offspring number and infection time, whereas plasticity allowed lower latent periods to reach larger burst sizes, dissimilarity reported in previous work that considered viral evolution only [11].

The presence or absence of the *B*-*L* tradeoff leads to an opposite interdependence of emergent burst size and host size (S3 Fig in S1 File, right): while the nonplastic case shows a negative correlation, the plastic case leads to a subtle positive correlation (non-monotonic for lower nutrient input N_0). For the nonplastic case, this decline results from a decreasing assembly period (difference between the values for the emerging latent period L and the fixed eclipse period E, see S4 Fig in S1 File left); for the plastic case, the decreasing assembly period (in this case defined as the difference between the emerging L and the E value set by the dominant host) is compensated by the increasing maturation rate as the dilution rate w increases.

Removing the "superinfection avoidance" term in Eq (3) and setting a viral extinction threshold that ignores intracellular viruses and focuses on free viruses only (see Methods) did not alter qualitatively the results of the model with plasticity (S5 Fig in S1 File).

Finally, we measured how the strategies above materialized in host, virus, and nutrient concentrations. The average nutrient concentration at stationarity was only noticeably impacted by the host only when both dilution rate w and input concentration N_0 were low (S4 Fig in S1 File, right), with hosts drawing down nutrient to lower levels in the plastic case. The density of the dominant host showed a nonmonotonic dependence on w, reaching a minimum for intermediate dilution rates (Fig 4, left). Differences in host density across nutrient input concentrations were barely noticeable for low w, small for large w, but large for intermediate w (e.g. more than an order of magnitude between the $N_0 = 5 \cdot 10^{-6}\ mol \cdot l^{-1}$ and $N_0 = 5 \cdot 10^{-5}\ mol \cdot l^{-1}$ cases). The average density of the dominant virus showed an overall decreasing trend with both dilution rate for high input concentration, and for the nonplastic case (Fig 4, right). In

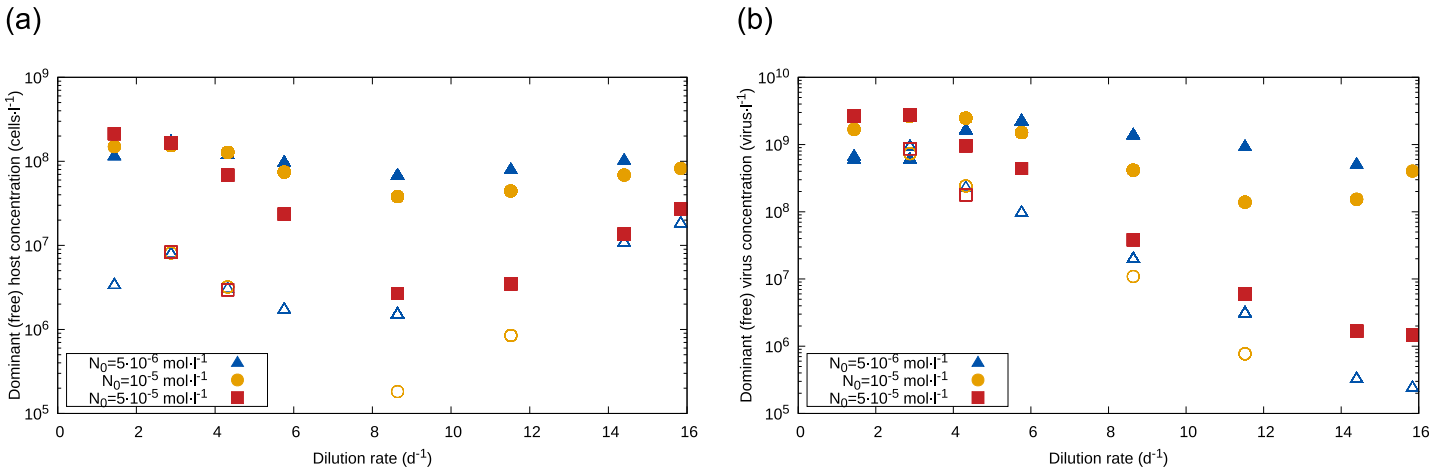

Fig 4. Density of the dominant population as a function of the dilution rate, *w*. Left: The concentration of the dominant host, averaged across replicates, initially decreased then increased, with a minimum value observed for intermediate w; concentrations were smaller for higher N_0 and the nonplastic case. Right: The concentration of the dominant viral phenotype decreased with w for high nutrient input and the nonplastic case, but remained within the 10^8—$5 \cdot 10^9\ cell \cdot l^{-1}$ range for lower N_0. Full symbols represent the plastic case, and open symbols the nonplastic case.

https://doi.org/10.1371/journal.pone.0268596.g004

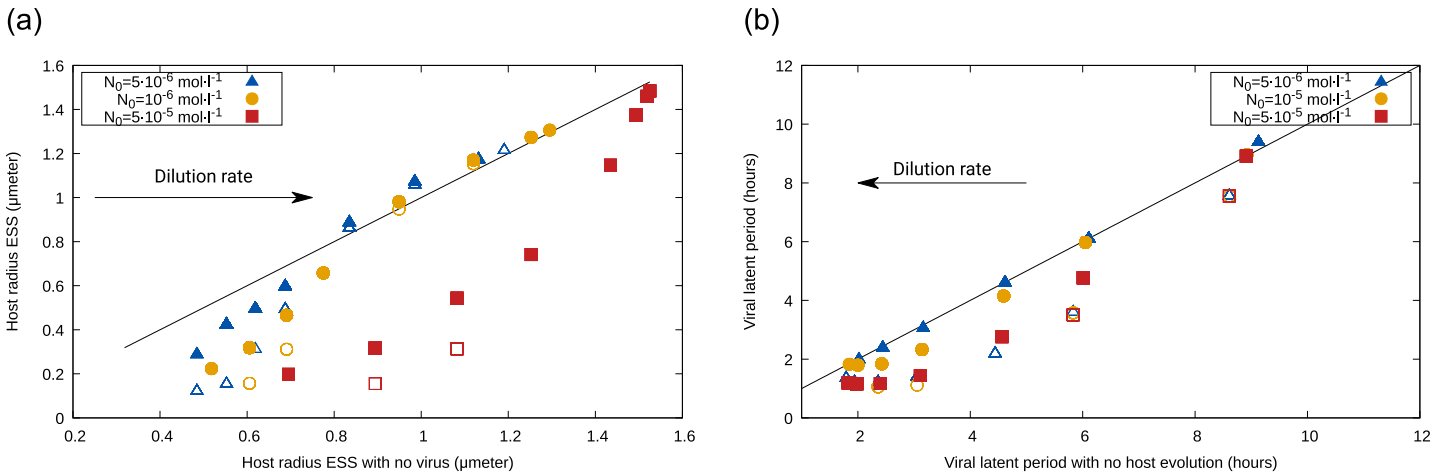

Fig 5. Left: Comparison between the host radius emerging from evolution with and without the virus; discrepancies (departures from the 1:1 line) occur for low dilution rates and for high nutrient input concentrations. Right: Comparison between the latent period emerging from coevolution with the host versus minimization of a fixed-radius host; differences occur for high w, and are accentuated by N_0 in the plastic case only. As before, full symbols represent the plastic case, and open symbols the nonplastic case.

https://doi.org/10.1371/journal.pone.0268596.g005

the plastic case, lower N_0 led to a more complicated pattern, with nonmonotonic changes that remained within the range 10^8—$5 \cdot 10^9$ $cell \cdot l^{-1}$ for all w.

Single evolution

The sizes emerging in the presence of the virus were positively correlated with those emerging in the absence of it, and the range of dilution rates for which departures from the 1:1 line (i.e. differences between the r_{ESS} with or without the virus) occur depended on the input concentration (Fig 5, left). While, for low N_0, departures were constrained to low dilution rates, for high N_0 differences occurred for any w. In all cases in which there were differences, hosts in the presence of the virus were smaller than in the absence of it.

For the latent period, high dilution rates led to shorter infections than in the absence of host evolution (the latter calculated as $L_{nocoev} = 1/w_{out} + E(\mu)$, see S1 File and [11, 28, 45]), but differences decreased as dilution or input concentration decreased (Fig 5, right). For any input concentration, the nonplastic case curve was similar to that of the high-N_0 plastic case.

Evolutionary collapse

As mentioned above, the number of replicates that resulted in extinction decreased with the input concentration for the plastic case and increased for the nonplastic case. We observed artificial (early) extinctions (see Methods) for almost all combinations of dilution rates and nutrient input concentrations, and only in a reduced number of cases extinctions occurred after the minimum 1, 000 days we set to discern whether the collapse resulted from the evolutionary process.

In these cases of evolutionary collapse, the host went to extinction before the virus, thus leading to the eventual collapse of the whole system. In this evolutionary path to extinction, the host seemed to be approaching the ESS corresponding to the case without the virus, while the virus was still evolving after starting from an initial phenotype with a high latent period L (S6 Fig in S1 File). The sizes of the host phenotypes that were present immediately before extinction showed a negative correlation with the latent period of the dominant virus (S7 Fig in S1 File). The correlation was less marked in the plastic case (left panel) than for the

nonplastic case (right). For the latter, the negative correlation was only broken for low sizes. For the former, mid-to-low sizes led to evolutionary collapse for a well-defined range of r (0.6–0.7 in S7 Fig in S1 File) but a much wider range of mid-to-high L ($\approx 20h$ in the example).

Discussion

The vast numbers and short generation time of microbial organisms, as well as the possibility of rapidly changing environments, emphasizes the importance of theories that take into account the overlapping effects of ecological and evolutionary responses to describe the dynamics of these organisms. A reliable description of the interaction between bacteria and phages thus requires accounting for coevolutionary responses as well as the effect that changes in host physiology has on the main traits characterizing viral performance (viral plasticity).

In previous work, we explored such coevolution by focusing on host size and viral latent period as evolving traits, constraining our study to cases in which both host and virus coexisted and showed an evolutionarily stable strategy (ESS) [14]. Here, we sought to eliminate any such constraints and study any outcome of this coevolutionary process, including potential evolutionary branching and extinction. One of such constraints was the use of an infinitesimal evolutionary step [52]; the larger standard deviations σ_r and σ_L used here enabled a more thorough exploration of the trait space while keeping a reasonable phenotypic link between offspring and parent. Some of the different results observed here may thus result from the new framework being able to find global evolutionary attractors and elude "evolutionary traps" (local attractors with deep basins of attraction). In addition, we sought to increase the stability of the system and reduce collapses not driven by evolution but instead by the random initial condition. To this end, we included viral superinfection avoidance, commonly observed for phages [29], through a density-dependent competition-like term in Eq (3) that reduced the amplitude of demographic oscillations. Moreover, we considered intracellular viruses when assessing whether a phenotype fell below the extinction threshold, which prevented the removal of viral phenotypes before their first latent period ends. Finally, we used here a more strict implementation of the classic (i.e. nonplastic) case that ensured that each viral phenotype's traits were fixed at all times regardless of the host.

Fig 6 summarizes the phenomenology we observed with our framework, and the mechanisms we hypothesize below underlie those observations.

Host-virus coexistence

The unconstrained evolution described by the new version of the model led to results similar to the previous version when host and virus coexisted [14], but also to important differences.

ESS and the absence of branching. Similarly to our previous study, the final stationary state was composed of a well-defined dominant phenotype for both host and virus. In other words, the system reached a well-defined ESS, with no instances of evolutionary branching. Nonetheless, the evolutionary path towards the ESS showed evolutionary leaps, more markedly observed for the host trait. Between leaps, distributions of the evolving traits were peaked but with a non-negligible width, with leaps being a transitory equalizing moment that enabled less-peaked distributions [53]. As expected, the evolutionary path towards the ESS in the current study showed a much wider degree of variation for both host and virus traits. Also differently, in the new version of the model plasticity led to larger infection times than when viral traits were fixed (nonplastic case), which results from parametrizing the latter strictly using values corresponding to the best possible physiological state that any host can show (i.e. $\mu = \mu_{max_{ref}}$) thus leading to the shortest possible latent periods.

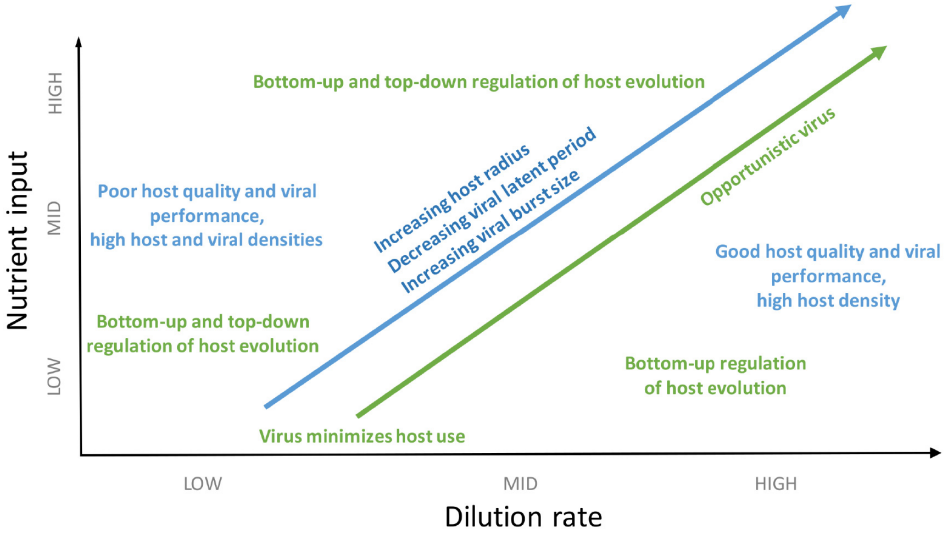

Fig 6. Schematic figure summarizing the phenomenology observed in the plastic case (blue tones) and hypothesized underlying mechanisms (green tones) as environmental conditions, represented by nutrient input concentration (vertical axis) and dilution rate (horizontal axis), change.

https://doi.org/10.1371/journal.pone.0268596.g006

Emergence and consequences of a negative correlation between host size and viral latent period. As in [14], the emergent host size was inversely correlated with the emergent viral latent period, that is, smaller hosts selected for longer infections. Moreover, the potential evolutionary payoffs for these strategies also depended on environmental conditions. For example, both plastic and nonplastic cases showed high host and virus population densities at low dilution rates. In both cases, low w led to lower nutrient availability and growth. The host lower growth associated with lower w selected for smaller cell sizes, which experienced reduced viral adsorption (Eq (7)) [35]. This strategy allowed the host to reach high density levels, aided by the evolutionary strategy for the virus (increasing the duration of infection). The (classic) positive dependence between burst size and latent period observed for the nonplastic case, however, led to an increased viral pressure that in turn resulted in high viral densities at the expense of the host population; as a result, the host showed lower densities than in the plastic case. For the latter, the fact that plasticity breaks the classic burst size-latent period (B-L) tradeoff means that the virus did not produce as much offspring per infection for low dilution, but the resulting increase in host density still enabled high viral densities; therefore, counterintuitively, due to viral plasticity, poor-growth conditions led to higher densities for both host and virus than in high-growth conditions [11]. The situation was maintained by a feedback loop in which increased host density led to lower nutrient availability and consequently host growth, decreasing viral performance and thus allowing for high host densities.

As the dilution rate increased, host size, growth, and adsorption all increased and allowed for shorter infections, which led to a lower host density. Although the burst size decreased for the nonplastic case and slightly increased for the plastic case, in both cases the viral population also decreased, which points to host availability (and not quality) driving this behavior. This decrease continued for the nonplastic case as w increased, as both latent period L and burst size B reached a lower value and thus the increase in dilution was not countered by an increase in viral production; instead, increased dilution led to a decrease in viral density that in turn enabled an increase in host density for high dilution rates. For the plastic case, the latent period also reached a lower value but the increasing host growth enabled a higher burst size; as a

result, the viral population increased with dilution for mid-to-low input concentration N_0, whereas the lower burst size B observed for high nutrient input led to a continuous decrease in viral availability. This lower viral density for high w and N_0 does not result from the superinfection avoidance term, since similar behavior was observed for a version of the model without it (i.e. for $\alpha_V = 0$, not shown). Host availability increased as dilution rate increased due to the improved growth conditions despite the improved viral performance, although higher input concentrations led to lower host densities as infection times shortened.

In summary, both plastic and nonplastic cases showed a convex dependence of host density on dilution, with a minimum of host availability for intermediate dilution rates resulting from the balance between bottom-up and top-down pressures. This minimum was thus not plasticity-driven, although accounting for plasticity led to higher host and viral densities.

Coevolution vs single evolution

Coevolution leads to smaller hosts in challenging conditions. The convex trait curves comparing the outcome of coevolution with instances of single evolution obtained with this version of the model were in contrast with the concave curves obtained with the previous version [14]. The fact that the cell size emerging from the coevolution with the virus transitioned from lower than to similar to the r_{ESS} obtained in the absence of the virus as dilution increased means that, under low-growth conditions, the outcome of host evolution was regulated by both nutrient availability and viral pressure; however, under high-growth conditions, top-down regulation played no significant evolutionary role. Nonetheless, high input concentrations led to very large hosts in the absence of the virus, strategy that in the presence of the virus exposes the host to viral infection but increases host maximum growth rate under decreased competition for resources (i.e. higher top-down and reduced bottom-up pressures); in this case, host evolution was thus both bottom-up and top-down regulated for any dilution rate w. On the other hand, the convexity of the host density curve results from the eco-evolutionary dynamics with the virus, since the curve is instead concave in the absence of the virus (not shown).

Coevolution shortens virus infections. For the virus, coevolution played an increasingly important role and shortened the emerging latent period as dilution rate and nutrient input increased. Given that the value in the absence of host coevolution, L_{nocoev}, represents the latent period that "minimizes resources" for the virus, the departure from the 1:1 line indicates that other evolutionary strategies were prioritized by the virus under those environmental conditions. The dependence on dilution may stem from a shift from host availability dominating the viral evolutionary strategy when w is low, to host size and growth rate being the main influencing factor as w increases. This hypothesis is reinforced by the sensitivity of the curve to the input concentration N_0 for high dilution rates observed only for the plastic case. For high nutrient input levels, the latent periods emerging for plastic and nonplastic cases agreed, as host growth remained around its maximum across dilution rates and thus any plastic viral trait remained effectively fixed. Another relevant factor to consider is that for high nutrient levels, and for the nonplastic case, demographic oscillations are more marked and thus the most suitable viral strategy may not be the one that prioritizes the minimization of resources but one accounting for the changing environment, which has been observed in microbes such as phytoplankton [54].

Evolutionary collapses result from a "complacent" host

The modifications implemented in the new version of the model enabled more dynamical stability than previous iterations [13, 14], as fewer initial conditions led to artificial (early) extinctions.

In addition to these early extinctions, we also observed evolutionary collapses. In these cases, the host population collapsed first, followed by the viral population. Also common to these cases, the initial random viral phenotype showed a high latent period ($L > 1\ d$) and the sequence of dominant phenotypes was approaching a lower L at the moment of host extinction. Given the proximity of the host size before extinction to the r_{ESS} reached without the virus, which we observed for many of these replicates, we speculate that extinction resulted from the host not being able to respond to changes in top-down regulation in a timely manner. The long infection times eased the evolutionary pressure on the host and, as a result, its evolving trait targeted the value expected under bottom-up regulation alone (i.e. virus not influencing host evolution). As host and virus evolved, infection time decreased, increasing mortality on the host, which could not adapt fast enough to the environmental changes and went extinct. This hypothesis is reinforced by the fact that increasing the dilution rate led to lower L values dominating at the moment of extinction: higher dilution means that the abiotic component of the environment exerts a higher pressure on the host and, therefore, lysis time needs to be smaller for the mortality rate due to lysis to become important for host dynamics. In the plastic case, the situation may be exacerbated by high growth rates from the dominant host guaranteeing high burst sizes for the virus. The evolutionary collapse is in this case a combination of an "evolutionarily underperforming" host and an "ecologically overachieving" (plastic) virus.

All instances of coexistence showed a more parsimonious evolutionary path in which the initial viral phenotype showed a lower latent period regardless of the initial value of host size, although a low initial L did not guarantee eventual coexistence as random initial extinctions were still possible.

Wider implications

Our broader study of the coevolution of host size and viral latent period under chemostat conditions has confirmed that increasing dilution rates select for larger cell sizes and smaller latent periods, which is in agreement with the observation that better host quality and availability select for shorter infections [5, 55]. In our plastic description, these conditions also mean higher burst size, thus confirming biologically plausible strategies for both host and virus. For oligotrophic conditions, evolution leads to smaller host sizes that reduce viral adsorption, and a longer infection time allows the virus to compensate the handicapped host physiology by enabling the recovery of host density between infections. For eutrophic conditions, both host and virus can switch to more opportunistic strategies, with larger and faster-growing cells that allow the host population to survive even with the accompanying high adsorption rates, and with short and very productive lytic cycles that the virus can sustain thanks to the high host growth.

The information above helps understand the factors that regulate microbial communities. The flows present in a chemostat can roughly represent a volume of water in the ocean (with advection moving nutrients, microbes, and viruses in and out of the focal volume, and turbulence mixing the medium), or the directional flows present in the intestinal tract. The gut microbiome, for example, would be an example of high nutrient input and availability, and therefore our model predicts that the dominating sizes in the bacterial community in the absence of the virus would be much larger than in the presence of phage. This could be relevant for predicting the fate of a viral infection affecting the microbiome. A similar situation would apply to nutrient-rich parts of the oceans, like cold or coastal waters, or zones of upwelling. In oligotrophic environments, on the other hand, the expectation would be for microbial hosts to show smaller sizes than in the absence of viruses (e.g. lab cultures), prediction reinforced by the observed increased competitive ability of small cells when taking up nutrients

[56, 57]. Our eco-evolutionary model is especially well-suited to describe dynamic situations, like pulses affecting host growth temporarily [58], or when the distribution of resources translates into a spatial dependence for host growth rate, like in biofilms [25] or for soil bacteria-virus systems [59].

The evolutionary collapses we observed may provide useful information for the use of phages to eliminate bacterial infections (phage therapy) [24]. Our results indicate that infecting a bacterial population with a virus with a long latent period would result in a coevolutionary path in which hosts adapt their size mostly to bottom-up pressures due to the long lysis times, and ultimately will not be able to survive the combination of high burst size (due to the high host growth rate) and decreasing infection times. Note that the initial time used here to filter pathological (i.e. unrealistically unstable) initial conditions would not be needed when considering naturally occurring host-virus systems. In our simulations, we did not observe replicates in which the viral population went extinct as a result of coevolution, although an alternative use of our model would be to predict how to use bacteria to eliminate viral infections.

These predictions could be tested with a comprehensive experiment that monitored the mid-to-long-term coevolution of host and virus, focusing on how host size and viral infection (offspring and duration) change over time and across environmental conditions. To the best of our knowledge, such an experiment does not exist. In addition to the obvious logistic challenges, one important factor complicating such an experiment is also a limitation of our framework: there are other potential targets for evolution in the system that may be subject to a higher pressure than host size and viral latent period. A situation that has been repeatedly studied in the past is the coevolutionary race that ensues when bacteria develop (total or partial) immunity against viral infection, and the virus tries to overcome such immunity [29, 60, 61]. One such examples is host avoidance of infection through a modification of LPS or other receptors, immunity that can be permanent or temporary depending on the viral capacity to, e.g. modify the tail fibers [50]. We are currently working on a version of the model that shifts the evolutionary focus towards changes in receptors by the host to avoid viral infection, and changes in host range by the virus that try to overcome such immunity and/or infect other host strains. We aim at understanding the role of plasticity in shaping this coevolutionary arms race.

The quantitative and qualitative differences observed here between the plastic and nonplastic versions of the model emphasize the need to consider plasticity in predictive theories for the eco-evolutionary dynamics of hosts and viruses. More empirical information is needed, however, to characterize viral plasticity in other important systems (e.g. different marine phytoplankton and virus species) and obtain the necessary expressions that unleash formalisms like the one presented here.

Supporting information

S1 File.
(PDF)

Acknowledgments

The authors would like to thank the anonymous reviewers of this and previous publications for helpful suggestions.

Author Contributions

Conceptualization: Juan A. Bonachela, Melinda Choua, Michael R. Heath.

Formal analysis: Juan A. Bonachela.

Funding acquisition: Juan A. Bonachela, Michael R. Heath.

Investigation: Juan A. Bonachela.

Methodology: Juan A. Bonachela.

Project administration: Juan A. Bonachela.

Writing – original draft: Juan A. Bonachela.

Writing – review & editing: Juan A. Bonachela, Melinda Choua, Michael R. Heath.

References

1. Suttle CA. Marine viruses—major players in the global ecosystem. Nature Reviews Micrbiology. 2007; 5:801–812. https://doi.org/10.1038/nrmicro1750 PMID: 17853907
2. Weinbauer MG. Ecology of prokaryotic viruses. FEMS Microbiol Rev. 2004; 28:127–181. https://doi.org/10.1016/j.femsre.2003.08.001 PMID: 15109783
3. Wang IN. Lysis timing and bacteriophage fitness. Genetics. 2006; 172:17–26. https://doi.org/10.1534/genetics.105.045922 PMID: 16219778
4. DeLong JP, Al-Sammak MA, Al-Ameeli ZT, et al. Towards an integrative view of virus phenotypes. Nat Rev Microbiol. 2021;. PMID: 34522049
5. Hadas H, Einav M, Fishov I, Zaritsky A. Bacteriophage T4 development depends on the physiology of its host Escherichia coli. Microbiol. 1997; 143:179–185. https://doi.org/10.1099/00221287-143-1-179 PMID: 9025292
6. You L, Suthers PF, Yin J. Effects of Escherichia coli Physiology on Growth of Phage T7 In Vivo and In Silico. J Bacteriol. 2002; 184:1888–1894. https://doi.org/10.1128/JB.184.7.1888-1894.2002 PMID: 11889095
7. Golec P, Karczewska-Golec J, Los M, Wegrzyn G. Bacteriophage T4 can produce progeny virions in extremely slow growing Escherichia coli host: comparison of a mathematical model with the experimental data. FEMS Microbiol Lett. 2014; 351:156–161. https://doi.org/10.1111/1574-6968.12372 PMID: 24386916
8. Webb V, Leduc E, Spiegelman GB. Burst size of bacteriophage SP82 as a function of growth rate of its host Bacillus subtilis. Can J Microbiol. 1982; 28:1277–1280. https://doi.org/10.1139/m82-190 PMID: 6185190
9. Birch EW, Ruggero NA, Covert MW. Determining Host Metabolic Limitations on Viral Replication via Integrated Modeling and Experimental Perturbation. PLoS Comput Biol. 2012; 8:e1002746. https://doi.org/10.1371/journal.pcbi.1002746 PMID: 23093930
10. Gnezda-Meijer K, Mahne I, Poljsak-Prijatelj M, Stopar D. Host physiological status determines phage-like particle distribution in the lysate. FEMS Microbiol Ecol. 2006; 55:136–145. https://doi.org/10.1111/j.1574-6941.2005.00008.x PMID: 16420622
11. Choua M, Bonachela JA. Ecological and Evolutionary Consequences of Viral Plasticity. Am Nat. 2019; 193:346–358. https://doi.org/10.1086/701668 PMID: 30794445
12. Weitz JS, Dushoff J. Alternative stable states in host-phage dynamics. Theoretical Ecology. 2008; 1:13–19. https://doi.org/10.1007/s12080-007-0001-1
13. Choua M, Heath MR, Speirs DC, Bonachela JA. The effect of viral plasticity on the persistence of host-virus systems. J Theor Biol. 2020; 498:110263. https://doi.org/10.1016/j.jtbi.2020.110263 PMID: 32333976
14. Choua M, Heath MR, Bonachela JA. Evolutionarily Stable Coevolution Between a Plastic Lytic Virus and Its Microbial Host. Front Microbiol. 2021; 12:63790. https://doi.org/10.3389/fmicb.2021.637490 PMID: 34093461
15. Edwards KF, Steward GF. Host traits drive viral life histories across phytoplankton viruses. Am Nat. 2018; 191:566–581. https://doi.org/10.1086/696849 PMID: 29693441
16. Lennon JT, Martiny JBH. Rapid evolution buffers ecosystem impacts of viruses in a microbial food web. Ecol Lett. 2008; 11:1178–1188. https://doi.org/10.1111/j.1461-0248.2008.01225.x PMID: 18647331
17. Pelletier F, Garant D, Hendry AP. Eco-evolutionary dynamics. Philos Trans R Soc Lond B Biol Sci. 2009; 364:1483–1489. https://doi.org/10.1098/rstb.2009.0027 PMID: 19414463

18. Litchman E, Klausmeier CA. Trait-Based Community Ecology of Phytoplankton. Annu Rev Ecol Evol Syst. 2008; 39:615–639. https://doi.org/10.1146/annurev.ecolsys.39.110707.173549

19. Bull JJ. Optimality models of phage life history and parallels in disease. J Theor Biol. 2006; 241:928–938. https://doi.org/10.1016/j.jtbi.2006.01.027 PMID: 16616205

20. Lehahn Y, Koren I, Schatz D, Frada M, Sheyn U, Boss E, et al. Decoupling Physical from Biological Processes to Assess the Impact of Viruses on a Mesoscale Algal Bloom. Current Biol. 2014; 24:2041–2046. https://doi.org/10.1016/j.cub.2014.07.046 PMID: 25155511

21. Vardi A, Haramaty L, Van Mooy BAS, Fredricks HF, Kimmance SA, Larsen A, et al. Host-virus dynamics and subcellular controls of cell fate in a natural coccolithophore population. Proc Natl Acad Sci USA. 2012; 109:19327–19332. https://doi.org/10.1073/pnas.1208895109 PMID: 23134731

22. Collins JR, Edwards BR, Thamatrakoln K, Ossolinski JE, DiTullio GR, Bidle KD, et al. The multiple fates of sinking particles in the North Atlantic. Ocean Glob Biogeochem Cycles. 2015; 29:1471–1494. https://doi.org/10.1002/2014GB005037

23. Pourtois J, Tarnita CE, Bonachela JA. Impact of Lytic Phages on Phosphorus- vs. Nitrogen-Limited Marine Microbes. Front Microbiol. 2020; 11:221. https://doi.org/10.3389/fmicb.2020.00221 PMID: 32153528

24. Weld RJ, Butts C, Heinemann JA. Models of phage growth and their applicability to phage therapy. J Theor Biol. 2004; 227:1–11. https://doi.org/10.1016/S0022-5193(03)00262-5 PMID: 14969703

25. Bonachela JA, Nadell CD, Xavier JB, Levin SA. Universality in Bacterial Colonies. J Stat Phys. 2011; 144:303–315. https://doi.org/10.1007/s10955-011-0179-x

26. Martínez-García R, Nadell CD, Hartmann R, Drescher K, Bonachela JA. Cell adhesion and fluid flow jointly initiate biofilm genetic structure. PLoS Comp Biol. 2018; 14:e1006094. https://doi.org/10.1371/journal.pcbi.1006094

27. Levin BR, Stewart FM, Chao L. Resource-limited growth, competition, and predation: a model and experimental studies with bacteria and bacteriophage. Am Nat. 1977; 111:3–24. https://doi.org/10.1086/283134

28. Bonachela JA, Levin SA. Evolutionary Comparison Between Viral Lysis Rate and Latent Period. J Theor Biol. 2014; 345:32–42. https://doi.org/10.1016/j.jtbi.2013.12.006 PMID: 24361326

29. van Houte S, Buckling A, Westra ER. Evolutionary Ecology of Prokaryotic Immune Mechanisms. Microbiol Mol Biol Rev. 2016; 80:745–763. https://doi.org/10.1128/MMBR.00011-16 PMID: 27412881

30. Monod J. Technique de Culture Continue. Theory et Applications. Ann Inst Pasteur. 1950; 79:390–410.

31. Chien AC, Hill NS, Levin PA. Cell size control in bacteria. Curr Biol. 2012; 22:R340–R349. https://doi.org/10.1016/j.cub.2012.02.032 PMID: 22575476

32. Yoshida M, Tsuru S, Hirata N, Seno S, Matsuda H, Ying BW. Directed evolution of cell size in Escherichia coli. BMC Evolutionary Biology. 2014; 14:257. https://doi.org/10.1186/s12862-014-0257-1 PMID: 25514845

33. Grant NA, Magid AA, Franklin J, Dufour Y, Lenski RE. Changes in Cell Size and Shape during 50,000 Generations of Experimental Evolution with Escherichia coli. J Bacteriol. 2021; 203:e00469–20. https://doi.org/10.1128/JB.00469-20 PMID: 33649147

34. Gallet R, Violle C, Fromin N, Jabbour-Zahab R, Enquist BJ, Lenormand T. The evolution of bacterial cell size: the internal diffusion-constraint hypothesis. ISME J. 2017; 11:1559–1568. https://doi.org/10.1038/ismej.2017.35 PMID: 28375214

35. Delbrück M. Adsoprtion of bacteriophage under various physiological conditions of the host. J Gen Physiol. 1940; 23:631–642. https://doi.org/10.1085/jgp.23.5.631 PMID: 19873179

36. Nikaido H, Vaara M. Molecular basis of bacterial outer membrane permeability. Microbiol Rev. 1985; 49:1–32. https://doi.org/10.1128/mr.49.1.1-32.1985 PMID: 2580220

37. Wirtz KW. A generic model for changes in microbial kinetic coefficients. J Biotechnol. 2002; 97:147–162. https://doi.org/10.1016/S0168-1656(02)00064-0 PMID: 12067521

38. Wortel M. Evolutionary coexistence in a fluctuating environment by specializationon resource level. bioRxiv. 2021;2021.05.18.444718:1–18.

39. Knowles B, Bonachela JA, Behrenfeld MJ, Bondoc KG, Cael BB, Carlson CA, et al. Temperate infection in a virus–host system previously known for virulent dynamics. Nature Communications. 2020; 11:1–13. https://doi.org/10.1038/s41467-020-18078-4

40. Herendeen SL, VanBogelen RA, Neidhardt FC. Levels of Major Proteins of Escherichia coli During Growth Proteins of Escherichia coli at Different Temperatures. J Bacteriol. 1979; 139:185–194. https://doi.org/10.1128/jb.139.1.185-194.1979 PMID: 156716

41. Schulze KL, Lipe RS. Relationship between Substrate Concentration, Growth Rate, and Respiration Rate of *Escherichia coli* in Continuous Culture. Archiv für Mikrobiologie. 1964; 48:1–20. https://doi.org/10.1007/BF00406595 PMID: 14196722

42. Fagerbakke KM, Heldal M, Norlan S. Content of carbon, nitrogen, oxygen, sulfur and phosphorus in native aquatic and cultured bacteria. Aquat Microbiol Ecol. 1996; 10:15–27. https://doi.org/10.3354/ame010015

43. De Paepe M, Taddei F. Viruses' Life History: Towards a Mechanistic Basis of a Trade-Off between Survival and Reproduction among Phages. PLOS Biology. 2006; 4:e193. https://doi.org/10.1371/journal.pbio.0040193 PMID: 16756387

44. Bull JJ, Millstein J, Orcutt J, Wichman HA. Evolutionary feedback mediated through population density, illustrated with viruses in chemostats. Am Nat. 2006; 167:E39–E51. https://doi.org/10.1086/499374 PMID: 16670974

45. Shao Y, Wang IN. Bacteriophage Adsorption Rate and Optimal Lysis Time. Genetics. 2008; 180:471–482. https://doi.org/10.1534/genetics.108.090100 PMID: 18757924

46. Weitz JS, Hartman H, Levin SA. Coevolutionary arms races between bacteria and bacteriophage. Proc Natl Acad Sci USA. 2005; 102:9535–9540. https://doi.org/10.1073/pnas.0504062102 PMID: 15976021

47. Menge DNL, Weitz JS. Dangerous Nutrients: Evolution of Phytoplankton Resource Uptake Subject to Virus Attack. J Theor Biol. 2009; 257:104–115. https://doi.org/10.1016/j.jtbi.2008.10.032 PMID: 19068219

48. Tilman D. Resource Competition and Community Structure. 1st ed. Princeton University Press; 1982.

49. Hall AR, Scanlan PD, Buckling A. Bacteria-phage coevolution and the emergence of generalist pathogens. Am Natural. 2011; 177:44–53. https://doi.org/10.1086/657441 PMID: 21117957

50. Bohannan BJM, Lenski RE. Linking genetic change to community evolution: insights from studies of bacteria and bacteriophage. Ecol Lett. 2000; 3:362–377. https://doi.org/10.1046/j.1461-0248.2000.00161.x

51. Levin S, editor. Fragile Dominion. 1st ed. Cambridge, MA: Perseus Publishing; 1999.

52. Dercole F, Rinaldi S. Analysis of Evolutionary Processes: The Adaptive Dynamics Approach and its Applications. Princeton, NJ: Princeton University Press; 2008.

53. Bonachela JA, Wortel M, Stenseth NC. Eco-evolutionary Red Queen dynamics regulate biodiversity in a metabolite-driven microbial system. Sci Rep. 2017; 7:17655–. https://doi.org/10.1038/s41598-017-17774-4 PMID: 29247226

54. Tozzi S, Schofield O, Falkowski P. Historical climate change and ocean turbulence as selective agents for two key phytoplankton functional groups. Mar Ecol Prog Ser. 2004; 274:123–132. https://doi.org/10.3354/meps274123

55. Abedon ST. Selection for Bacteriophage Latent Period Length by Bacterial Density: A Theoretical Examination. Microb Ecol. 1989; 18:79–88. https://doi.org/10.1007/BF02030117 PMID: 24196124

56. Ward BA, Marañón E, Sauterey B, Rault J, Claessen D. The size dependence of phytoplankton growth rates: a trade-off between nutrient uptake and metabolism. Am Nat. 2017; 189:170–177. https://doi.org/10.1086/689992 PMID: 28107051

57. Armstrong RA. Nutrient uptake rate as a function of cell size and surface transporter density: A Michaelis-like approximation to the model of Pasciak and Gavis. Deep-Sea Research I. 2008; 55:1311–1317. https://doi.org/10.1016/j.dsr.2008.05.004

58. Caceres C, Spatharis S, Kaiserli E, Smeti E, Flowers H, Bonachela JA. Temporal phosphate gradients reveal diverse acclimation responses in phytoplankton phosphate uptake. ISME J. 2019; 13:2834–2845. https://doi.org/10.1038/s41396-019-0473-1 PMID: 31350454

59. Emerson JB. Soil viruses: a new hope. mSystems. 2019; 4:e00120–19. https://doi.org/10.1128/mSystems.00120-19 PMID: 31138723

60. Brockhurst BKMA. Bacteria–phage coevolution as a driver of ecological and evolutionary processes in microbial communities. FEMS Microbiol Rev 3. 2014; 38:916–931. https://doi.org/10.1111/1574-6976.12072 PMID: 24617569

61. Dy R. L. and Richter C. and Salmond G. P. C. and Fineran P. C. Remarkable Mechanisms in Microbes to Resist Phage Infections. Annu Rev Virol. 2014; 1:307–331. https://doi.org/10.1146/annurev-virology-031413-085500 PMID: 26958724